Phase optimization of dispersive mirrors based on floating constants

M. K. Trubetskov,[1,*] V. Pervak,[2] and A. V. Tikhonravov[1]

[1]*Research Computing Center, Moscow State University, Leninskie Gory, 119992 Moscow, Russia*
[2]*Ludwig-Maximilians-Universitaet Muenchen, Am Coulombwall 1, D-85748 Garching, Germany*
*trub@srcc.msu.ru

Abstract: A novel floating constants phase-optimization technique is developed and applied to the design of dispersive mirrors. This technique reduces the dispersive mirror's sensitivity to layer thickness errors. To demonstrate the significant improvement in design stability, we theoretically and experimentally compare our new phase-optimization approach to the conventional one. The fabricated dispersive mirror has a reflectivity of >99.99% and provides an accurate dispersion control over a bandwidth of around 60 nm.

©2010 Optical Society of America

OCIS codes: (310.4165) Multilayer design, (310.1620) Interference coatings, (320.7160) Ultrafast technology

---

References and links

1. R. Szipöcs, K. Ferencz, C. Spielmann, and F. Krausz, "Chirped multilayer coatings for broadband dispersion control in femtosecond lasers," Opt. Lett. **19**(3), 201–203 (1994).
2. F. X. Kärtner, U. Morgner, R. Ell, T. Schibli, J. G. Fujimoto, E. P. Ippen, V. Scheuer, G. Angelow, and T. Tschudi, "Ultrabroadband double-chirped mirror pairs for generation of octave spectra," J. Opt. Soc. Am. B **18**(6), 882–885 (2001).
3. G. Steinmeyer, "Femtosecond dispersion compensation with multilayer coatings: toward the optical octave," Appl. Opt. **45**(7), 1484–1490 (2006).
4. G. Steinmeyer, and G. Stibenz, "Generation of sub-4-fs pulses via compression of a white-light continuum using only chirped mirrors," Appl. Phys. B **82**(2), 175–181 (2006).
5. N. Matuschek, L. Gallmann, D. H. Sutter, G. Steinmeyer, and U. Keller, "Back-side-coated chirped mirrors with ultra-smooth broadband dispersion characteristics," Appl. Phys. B **71**(4), 509–522 (2000).
6. G. Steinmeyer, "Brewster-angled chirped mirrors for high-fidelity dispersion compensation and bandwidth exceeding one optical octave," Opt. Express **11**(19), 2385–2396 (2003).
7. D. Strickland, and G. Mourou, "Compression of amplified chirped optical pulses," Opt. Commun. **56**(3), 219–221 (1985).
8. A. Ashkin, G. D. Boyd, and J. M. Dziedzic, "Resonant optical second harmonic generation and mixing," IEEE J. Quantum Electron. **2**(6), 109–124 (1966).
9. P. Tournois, "Acousto-optic programmable dispersive filter for adaptive compensation of group delay time dispersion in laser systems," Opt. Commun. **140**(4-6), 245–249 (1997).
10. A. V. Tikhonravov, M. K. Trubetskov, and A. A. Tikhonravov, "To the design and theory of chirped mirrors," In *Optical Interference Coatings* **9**, OSA Technical Digest Series, 293–295, (Optical Society of America, Washington DC, 1998).
11. M. Trubetskov, "Design of dispersive mirrors for ultrafast applications," Chin. Opt. Lett. **8**(S1), 12–17 (2010).
12. A. V. Tikhonravov, M. K. Trubetskov, and G. W. DeBell, "Application of the needle optimization technique to the design of optical coatings," Appl. Opt. **35**(28), 5493–5508 (1996).
13. A. V. Tikhonravov, M. K. Trubetskov, and G. W. DeBell, "Optical coating design approaches based on the needle optimization technique," Appl. Opt. **46**(5), 704–710 (2007).
14. A. V. Tikhonravov, and M. K. Trubetskov, OptiLayer Thin Film Software, *http://www.optilayer.com*
15. A. O'Keefe, and D. A. G. Deacon, "Cavity ring-down Optical Spectrometer for absorption measurements using pulsed laser sources," Rev. Sci. Instrum. **59**(12), 2544 (1988).
16. P. Zalicki, and R. N. Zare, "Cavity ring-down spectroscopy for quantitative absorption measurements," J. Chem. Phys. **102**(7), 2708–2717 (1995).
17. G. Berden, R. Peeters, and G. Meijer, "Cavity ring-down spectroscopy: Experimental schemes and applications," Int. Rev. Phys. Chem. **19**(4), 565–607 (2000).

18. T. V. Amotchkina, A. V. Tikhonravov, M. K. Trubetskov, D. Grupe, A. Apolonski, and V. Pervak, "Measurement of group delay of dispersive mirrors with white-light interferometer," Appl. Opt. **48**(5), 949–956 (2009).

1. Introduction

For over a decade, dispersive mirrors (DM) [1–6] have been playing an important role in the dispersion compensation of femtosecond lasers, as they possess low losses and well-controlled dispersion. Nowadays, requirements of precise dispersion compensation in laser systems are higher than before due to the increased complexity and improved performance of such systems. Furthermore, a high mirror reflectivity has to be maintained in a broader spectral range to support shorter pulses. Many applications like chirped pulse amplification (CPA) [7] and enhancement cavities [8] require the residual oscillation compensation with a high precision in order to produce pulses close to their Fourier limits. In the case of CPA, one can use an acousto-optic programmable dispersive filter [9] (DAZZLER) which provides effective dispersion control. DAZZLER is expensive and has a relatively low damage threshold due to the absorption by an acousto-optic crystal. For high-energy systems, we propose to use DM's that are highly tailored to a final tune of a phase. Although DM's can support higher pulse energy, their group delay dispersion (GDD) cannot be changed after their fabrication, unlike DAZZLER. Nevertheless, DM's can be successfully used for the final phase tuning in laser systems when additional phase adjustments are not required. Unfortunately, the accuracy of the modern thin-film technology is not sufficient for fabrication of DM's having the required residual phase compensation because of a high sensitivity of the DM's dispersion characteristics with respect to deviations in layer thicknesses.

At present, the level of precision of layer deposition technology is sufficient to provide an layer thickness accuracy of about 0.5-1.0 nm for the magnetron-sputtering and ion-beam-sputtering techniques. This means that, for compensating dispersion with a multilayer DM, one should be able to find a design having acceptably small variations of all spectral characteristics, including GDD, and thickness errors no larger than 0.5-1.0 nm.

In Ref. [10], a special algorithm for designing DM's was proposed. This algorithm deals directly with target phase characteristics as opposed to the conventional group delay (GD) and GDD targets. It turns out that operating directly with phase targets allows one to obtain designs that are less sensitive to deviations of layer thicknesses. Using one such design, we were able to fabricate a DM which provides accurate dispersion control over a bandwidth of around 60nm, which was previously impossible to achieve using designs obtained with the conventional GD and GDD targets approaches. The fabricated DM also has a high reflectivity of >99.99%.

2. Phase optimization approach

The phase optimization approach considered in this section is a further development of the design approach proposed in Ref. [10]. Typically, a DM design goal is specified using the reflectivity and GD or GDD targets. Merit functions constructed on the basis of GD and GDD targets are difficult for optimization due the extremely high sensitivity of GD and GDD with respect to variations in the layer thicknesses. In most cases, GD and GDD fluctuations — which are always present due to interface mismatch of top layer and incidence medium, force an optimization algorithm to increase the design's total optical thickness and its total number of layers. Thus, if the problem can be reformulated so that the optimization algorithm is less sensitive to the GD and GDD fluctuations, then its computational efficiency can be drastically increased. To reach this goal, we propose using a phase target instead of GD and GDD targets.

The phase introduced by a DM can be calculated from its GDD with the introduction of two integration constants C_1 and C_2:

$$\hat{\varphi}(\omega) = \int\limits_{\omega_0}^{\omega} d\omega_1 \int\limits_{\omega_0}^{\omega_1} \mathrm{GDD}(\omega_2)\, d\omega_2 + C_1\omega + C_2\,. \tag{1}$$

By optimizing with respect to the phase target, as opposed to the GDD target, we now end up with two additional parameters: floating constants C_1 and C_2. The resulting merit function can be expressed as

$$F(\mathbf{X}, C_1, C_2) = \frac{1}{L}\sum_{m=1}^{L}\left[\left(\frac{R(\lambda_m) - R^{(m)}}{\Delta R^{(m)}}\right)^2 + \left(\frac{\varphi(\lambda_m) - \varphi^{(m)}}{\Delta\varphi^{(m)}}\right)^2\right], \tag{2}$$

where $\mathbf{X} = \{d_k\}$ is the vector of layer thicknesses, $R(\lambda_m)$ and $\varphi(\lambda_m)$ are theoretical reflectances and phases on reflection, $R^{(m)}$ and $\varphi^{(m)}$ are target values, $\Delta R^{(m)}$ and $\Delta\varphi^{(m)}$ are tolerances, represented on a wavelength grid defined by λ_m, $m = 1,\dots,L$. The phase target values $\varphi^{(m)} = \hat{\varphi}(\omega_m)$ are defined according to Eq. (1) and therefore depend on the floating constants C_1 and C_2.

Optimization of the merit function Eq. (2) was first proposed in [10], where integration constants were chosen by a trial-and-error method. A yet more advanced approach [11] is based on automated exclusion of these constants from the merit function Eq. (2). Indeed, it is clear that $F(\mathbf{X}, C_1, C_2)$ depends on the variables C_1 and C_2 quadratically. Thus, for any vector of thicknesses $\mathbf{X}$ there exists a unique combination of C_1^* and C_2^* yielding a minimal value of $F(\mathbf{X}, C_1, C_2)$. The values C_1^* and C_2^* are determined analytically as solutions of a system of linear first-order differential equations

$$\partial F(\mathbf{X}, C_1, C_2)/\partial C_1 = 0, \quad \partial F(\mathbf{X}, C_1, C_2)/\partial C_2 = 0. \tag{3}$$

Therefore, it is possible to exclude these constants from the optimization problem, thereby reducing the optimization problem to a form that is amenable to the application of needle optimization [12,13]. During this reduction, it is necessary to take into account that the floating constants C_1^* and C_2^* are implicit functions of the vector $\mathbf{X}$. As well, expressions for the merit function's gradient and the perturbation function of the needle optimization method [12,13] become more complicated. We call this approach *needle optimization with floating constants*. The phase optimization approach with floating constants has since been implemented as an additional plug-in module to the OptiLayer software package [14].

3. Comparison of phase optimization approach and conventional design approaches

To demonstrate the efficiency of the floating constants phase designing approach, we compensated for the dispersion due to an imperfection of another DM that was used to compensate for glass and sapphire plate dispersions in a laser system.

We begin by describing the design of the DM using the conventional technique, i.e. by first formulating the design target in terms of a wavelength dependence of its GDD. This GDD target oscillates around zero with an amplitude up to 35 fs^2, and almost coincides with the blue curve at the right pane of Fig. 1. As an additional optimization target, we sought a high reflection in the wavelength range from 760 to 820 nm. We performed the optimization with OptiLayer software [14] using conventional needle optimization and gradual evolution synthesis techniques [12,13]. This design will be referred below as the *conventional* DM design.

Figure 1 (left pane, blue curve) shows that the level of DM transmittance we obtained is very low in this wavelength region. As a result, the designed DM has a high reflectivity

>99.99% in the range 760-820 nm. The theoretical GDD values of the conventional design are shown in Fig. 1, for normal incidence (right pane, blue curve) and for 10° incidence with p-polarization (magenta curve). The theoretical GDD almost coincides with the target GDD in this case, thus the target GDD is not shown in Fig. 1.
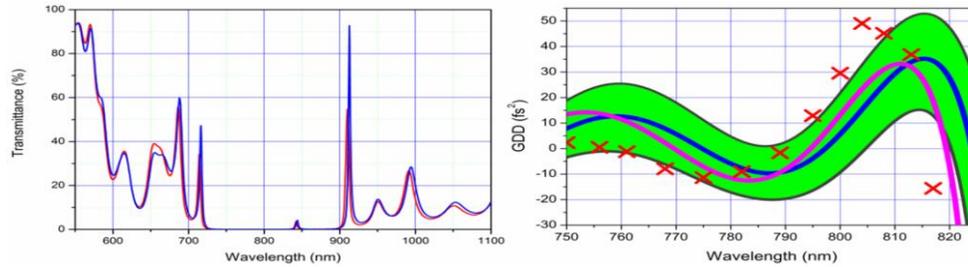

Fig. 1. The theoretical (blue curve) and measured (red curve) transmittances of the conventional DM are shown in the left pane. In the right pane, the theoretical GDD at normal incidence (blue curve) and the theoretical GDD at 10° incidence with p-polarization (magenta curve) of the conventional DM are shown. Red crosses correspond to GDD measured with a white light interferometer (10° incidence, p-polarization). The green area shows a 68.3% probability corridor of GDD errors obtained by Monte-Carlo analysis.

The conventional design consists of 51 alternating Ta_2O_5/SiO_2 layers. The design structure is shown in the left pane of Fig. 2, layers are counted from the substrate to incident medium.
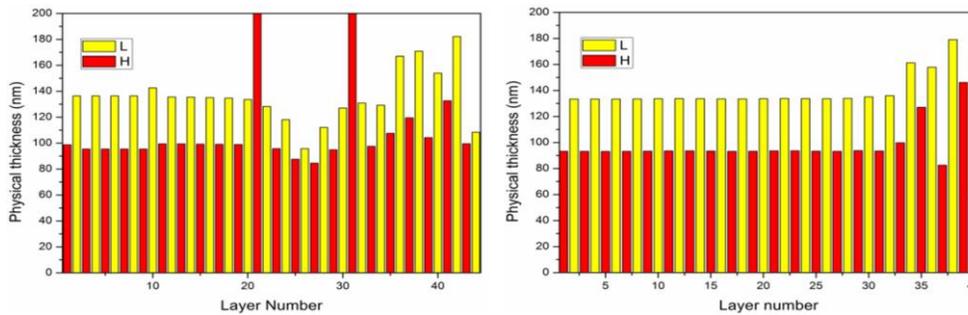

Fig. 2. Design structures of the DM designed by the conventional (left) and phase optimization (right) approaches.

Applying the new floating constants phase optimization approach, we were able to obtain a design consisting of 40 layers, i.e. 11 layers less than in the conventional design. The structure of the new design is shown in the right pane of Fig. 2. The design structure looks similar to a quarter-wave stack with only a few of the last layers modified. It is worth noting here that quarter-wave stacks usually demonstrate relatively low sensitivity to deposition errors. This design will be referred to below as the *phase-optimized* DM design.

The sensitivity of DM to manufacturing errors was estimated with a Monte-Carlo error analysis procedure. We added normally distributed errors with zero mean and a standard deviation of 1 nm to layer thicknesses and recalculated the dispersion properties 100 times. Our statistical analysis of GDD values yielded a 68.3% probability corridor of errors, i.e., the area where GDD values belong with the probability 68.3%. This corridor is shown in the right panes of Figs. 1 and 3 as a green area. Clearly, the width of the error corridor is significantly smaller for the phase-optimized design. As a result, we expect a much more robust and reproducible manufacturing of these phase-optimized designs. This is experimentally demonstrated in the following.

Both DMs were deposited on fused silica superpolished substrates with magnetron-sputtering deposition process using a state-of-the-art coater (Helios, Leybold Optics GmbH, Alzenau, Germany). The measured transmission spectra of both DMs are rather close to

theoretical transmittances and are shown in the left panes of Fig. 1 and 3 by red curves. Additionally, we performed precise measurements of the reflectance of both DM's at 808 nm with a loss-meter based on a ring-down technology (Novawave) [15–17]. While both the conventional and the phase-optimized DM's have a reflectivity of > 99.99%, their dispersive properties are quite different.

The GDD of the deposited DM's was measured with white-light interferometer [18] at 10° incidence for *p*-polarization. Measured GDD values are shown in Figs. 1 and 3 by red crosses. They should be compared with theoretical GDD of the designed DMs at 10° incidence for *p*-polarization (magenta curves at right panes of Figs. 1 and 3).

The measured GDD clearly deviates significantly from theoretically predicted values for the conventional DM. This deviation was caused by errors in layer thicknesses during deposition. As the result, the conventional DM design did not provide us with GDD values close enough to target specifications. On the other hand, the phase-optimized DM yielded GDD values which are rather close to target specifications (Fig. 3, right pane), in spite of similar deposition conditions and thus similar expected values of deposition thickness errors.
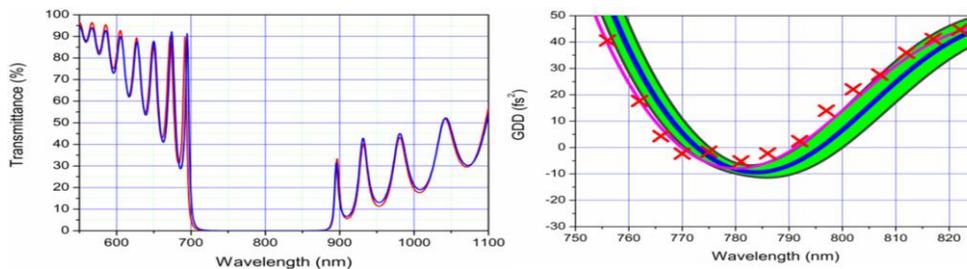

Fig. 3. The theoretical (blue curve) and measured (red curve) transmittances of the phase-optimized DM are shown in the left pane. In the right pane the theoretical GDD at normal incidence (blue curve) and the theoretical GDD at 10° incidence with *p*-polarization (magenta curve) of the phase-optimized DM are shown. Red crosses correspond to GDD measured with a white light interferometer (10° incidence, *p*-polarization). The green area shows 68.3% probability corridor of GDD errors obtained by Monte-Carlo analysis.

The GDD of the phase-optimized DM is different from that of the conventionally optimized DM, as illustrated in Fig. 4. This is because we converted GDD targets to phase targets. That is, by integrating the GDD we obtain two integration constants (floating constants) C_1 and C_2, which provide us with two additional degrees of freedom, allowing us to modify the formulated problem in such a way that we have a series of phase targets. Each set of C_1 and C_2 corresponds to a new phase curve. The algorithm thus automatically optimizes values of C_1 and C_2 during computations, and can actually change the optimization target during a design procedure. One can see that the phase curves shown in Fig. 4 (right) have similar behavior and differ only in the term $C_1\omega + C_2$. At the end of the optimization, we obtain solutions which have a GDD different (see Fig. 4, left pane) from each other due to invisible fluctuations in the phase curves around the desired value. The phase optimization approach enables the optimization algorithm to modify the target in such a way that the optimal compensation design is found.
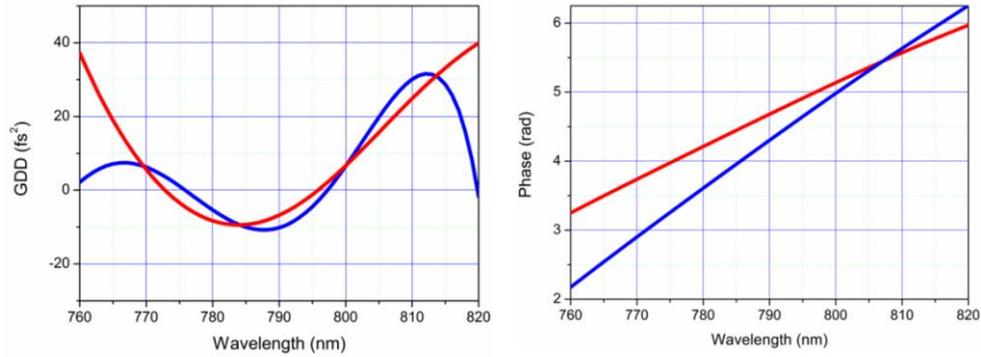
Fig. 4. Theoretical GDD values (left pane) and phases (right pane) of the conventional (blue lines) DM and phase-optimized (red lines) DM.

4. Conclusions

The phase-optimized DM demonstrates its superior performance in terms of precise residual dispersion compensation, which was impossible with the conventional dispersion target. This is possible due to a reduction of the design sensitivity to errors in layer thicknesses. The authors believe that the phase-optimization with floating constants technique can be successfully applied to multilayer coatings used in laser systems when precise phase compensation is required.

Acknowledgements